Deceleration of cell cycle underpins a switch from proliferative- to terminal division in plant stomatal lineage

Soon-Ki Han[1,2*], Jiyuan Yang[3,4], Machiko Arakawa[1], Rie Iwasaki[1], Tomoaki Sakamoto[5], Seisuke Kimura[5], Eun-Deok Kim[3,4], and Keiko U. Torii[1,3,4]

[1]Institute of Transformative Bio-Molecules (WPI-ITbM), Nagoya University, Nagoya, Aichi, 464-8601, Japan

[2]Institute for Advanced Research (IAR), Nagoya University, Nagoya, Aichi, 464-8601, Japan

[3]Howard Hughes Medical Institute, University of Texas at Austin, Austin, TX 78712 USA

[4]Department of Molecular Biosciences, University of Texas at Austin, Austin, TX 78712 USA

[5]Department of Industrial Life Sciences and Center for Plant Sciences, Kyoto Sangyo University, Kyoto-shi, Kyoto 603-8555, Japan

Correspondence: Keiko U. Torii, ktorii@utexas.edu

*Present address: Department of New Biology, DGIST (Daegu Gyeongbuk Institute of Science and Technology), Daegu 42988, Republic of Korea

ABSTRACT

Differentiation of specialized cell types from self-renewing progenitors requires precise cell cycle control. Plant stomata are generated through asymmetric divisions of a stem-cell-like precursor meristemoid followed by the single symmetric division that creates an adjustable pore surrounded by paired guard cells. The stomatal-lineage-specific transcription factor MUTE terminates the asymmetric divisions and triggers differentiation. However, the role of cell cycle machinery in this transition remains unknown. Through time-lapse imaging, we discover that the symmetric division is slower than the asymmetric division. We identify a plant-specific cyclin-dependent kinase inhibitor, SIAMESE-RELATED4 (SMR4), as a molecular brake that decelerates cell cycle during this transition. *SMR4* is directly induced by MUTE and transiently accumulates in differentiating meristemoids. SMR4 physically and functionally associates with CYCD3;1 and extends G1-phase of asymmetric divisions. By contrast, SMR4 fails to interact with CYCD5;1, a MUTE-induced G1 cyclin, and permits the symmetric division. Our work unravels a molecular framework of the proliferation-to-differentiation switch within the stomatal lineage and suggests that a timely proliferative cell cycle is critical for the stomatal fate specification.

INTRODUCTION

Growth and development of multicellular organisms rely on faithful cell-cycle progression, in which fundamental mechanism is highly conserved across the eukaryote kingdoms (Elledge, 1996; Harashima et al., 2013). Accumulating evidence in metazoans emphasizes that cell-cycle machinery is modulated during development, operating distinctly in proliferating stem cells vs. differentiating cells (Budirahardja and Gonczy, 2009). For example, early embryogenesis of flies, fish and frogs, as well as murine embryonic stem cells, execute rapid cell cycle mode due to shortened gap phases. As they undergo fate specification or differentiation, the duration of cell cycle increases (Coronado et al., 2013; Dalton, 2015; Liu et al., 2019). This phenomenon raises a major question regarding their causal relationships; whether the mode of cell cycle plays a role in maintaining pluripotency and whether changes in cell cycle upon dissolution of pluripotency drive fate specification or differentiation.

A typical eukaryotic cell cycle is composed of four distinct phases, G1-S-G2-M. Cell-cycle progression is driven by the oscillation of cyclin-dependent kinase (CDK) activity triggered by phase-specific cyclins, which are tightly regulated by the level of synthesis and proteolysis (Harashima et al., 2013; Morgan, 2007). CDK activity is negatively regulated by cyclin-dependent kinase inhibitors (CKIs). The G1/S transition is initiated by D-type Cyclin (CyclinD) and CDK complex, which relieve Retinoblastoma (Rb)-mediated repression on S-phase gene expression (Bertoli et al., 2013). Accumulating studies suggest that the G1 extension is indicative of differentiation (Coronado et al., 2013; Liu et al., 2019).

Plants possess a large number of genes encoding cyclins, CDKs, and CKIs (Inze and De Veylder, 2006). Studies have shown how specific cell cycle components are coupled to developmental patterning. For example, during Arabidopsis root development, transcription factors SHORTROOT and SCARECROW directly induce a D-type cyclin, CYCD6;1, that drives a formative cell division to create root endodermis and cortex cells (Sozzani et al., 2010). Another example is lateral root formation, in which auxin-induced formative division is modulated by CYCD2;1 and plant CKI, KIP-RELATED PROTEIN2 (KRP2, also known as ICK2) (Sanz et al., 2011). Some highly-specialized plant cell types, such as epidermal

69 pavement cells and trichomes, undergo endoreduplication at the onset of terminal
70 differentiation (Inze and De Veylder, 2006). Plant-specific CKIs, including SIAMESE (SIM) and
71 SIAMESE-RELATED1 (SMR1, also known as LGO) regulate morphogenesis of trichomes and
72 sepal giant cells, respectively, by promoting endoreduplication presumably via inhibiting CDK
73 activity (Hamdoun et al., 2016; Roeder et al., 2010; Walker et al., 2000). It remains unclear if
74 the modulation of cell cycle contributes to switching the cell division mode - from stem cell
75 divisions to differentiating cell divisions - in plants.

76 Development of stomata, valves on the plant aerial epidermis for gas exchange and
77 water control, is an accessible model of *de novo* initiation and differentiation of lineage-specific
78 stem cells. In Arabidopsis, birth of pores begins with the stomatal- lineage fate specification
79 of protodermal cells, which forms bipotent meristemoid mother cells (MMC) able to become
80 either stomata or pavement cells (Han and Torii, 2016; Lau and Bergmann, 2012). A series of
81 asymmetric cell division (ACD) follows to amplify the number of stomatal lineage precursor
82 cells, meristemoids and stomatal lineage ground cells (SLGC). The meristemoid renews itself
83 after ACD, thus behaving as a transient stem cell. After a few rounds of ACDs, a single round
84 of terminal symmetric cell division (SCD) of a guard mother cell (GMC) proceeds, completing
85 a stoma composed of paired guard cells (Han and Torii, 2016; Lau and Bergmann, 2012)
86 (Figure 1A).

87 Accumulating evidence supports that master-regulatory bHLH proteins SPEECHLESS
88 (SPCH), MUTE, and FAMA govern cell-state transitions within the stomatal lineage, in part via
89 directly regulating the expression of cell cycle genes (Adrian et al., 2015; Hachez et al., 2011;
90 Han et al., 2018; Lau et al., 2014) (Figure 1 A). SPCH initiates and sustains the ACDs of a
91 meristemoid in part via upregulating D-type cyclins CYCD3;1 and 3;2 (MacAlister et al., 2007;
92 Vaten et al., 2018). MUTE terminates proliferative cell state and drives final SCD by activating
93 a large subset of cell cycle regulators, including CYCD5;1 (Han et al., 2018; Pillitteri et al.,
94 2007). FAMA and a Myb protein, FOUR LIPS, are directly induced by MUTE and inhibit SCD
95 via direct suppression of the cell cycle genes, thereby ensuring that the SCD occurs just once
96 (Hachez et al., 2011; Han et al., 2018; Xie et al., 2010). However, it is not known how

97 proliferative ACD switches to terminal SCD, and whether the core cell cycle machinery
98 contributes to this process.

99 Through time-lapse imaging of stomatal development using plant cell cycle marker
100 PlaCCI (Desvoyes et al., 2020), we discovered that the stomatal SCD cycle is slower than that
101 of ACDs. Subsequent transcriptomic and ChIP-sequencing analyses identified that MUTE
102 directly induces the expression of *SMR4* during meristemoid-to-GMC transition. Through loss-
103 of-function and stomatal-lineage specific overexpression of SMR4 as well as its functional
104 interaction studies with D-type cyclins, we elucidate that SMR4 acts as a molecular brake to
105 decelerate cell cycle in G1 phase to ensure termination of the ACD cycle and facilitate faithful
106 progression to SCD. This SMR4 activity is distinct from canonical functions of SIM/SMR to
107 trigger endoreduplication. Taken together, we reveal a molecular framework of the cell
108 proliferation-to-differentiation switch within the stomatal lineage and suggest that a timely
109 proliferative ACD cycle is critical for differentiation of stomata with proper GC size, shape, and
110 identity.

111

112

113 **RESULTS**

114

115 **The single symmetric division of stomatal precursor is slower than amplifying**
116 **asymmetric division**

117 The stomatal precursor cells execute a unique transition from amplifying asymmetric cell
118 division (ACD) to a single symmetric cell division (SCD), a step coordinated by the bHLH
119 protein MUTE (Figure 1A). To understand if a switch from the ACD-to-SCD division mode links
120 to the cell cycle dynamics, we first performed time-lapse imaging of developing cotyledon
121 epidermis by using the multi-color plant cell cycle marker, PlaCCI (Desvoyes et al., 2020) and
122 examined each phases of cell cycle during asymmetric and symmetric divisions (Figure 1B-
123 D; Figure S1). The average cell cycle time of ACD of meristemoid and SCD of GMC was 8.63
124 ± 2.52 and 15.27 ± 4.73 hrs, respectively (Figure 1B), indicating that ACD is faster by ~7.5

125 hours than SCD that creates a pair of guard cells. Measuring cell division time using a plasma-
126 membrane marker LTI6b-GFP yielded essentially the same results (Figure S2). Duration of
127 each phase was extended in the SCD (Figure 1C). On the basis these findings, we conclude
128 that the switching from ACD to SCD involves cell cycle slow down.
129
130 ***SMR4* is expressed in stomatal-lineage cells and directly induced by MUTE**
131 In Eukaryotic cells, CKIs negatively regulate cell-cycle progression. To identify a factor that
132 plays a role in the decelerating cell cycle during the ACD-to-SCD transition, we surveyed
133 publicly-available transcriptome data (Han et al., 2018; Lau et al., 2014) to search for *CKIs*
134 that are induced by SPCH and MUTE. Among the 7 *KRP* and 17 *SIM* /*SMR* genes (Kumar
135 and Larkin, 2017; Peres et al., 2007), only *SMR4* exhibits marked increase by the induced
136 *MUTE* overexpression (*iMUTE*) (Figure 2A). On the other hand, a majority of *SMRs* and *KRPs*
137 is either downregulated or unchanged upon *iMUTE* or *iSPCH* (Figure 2A). Subsequently, we
138 performed time-course induction analysis. Consistent with the transcriptome data, *SMR4*
139 expression was increased by iMUTE with similar kinetics to a known direct MUTE target, *TMM*
140 (Han et al., 2018) (Figure 2B). In addition, iMUTE induced *SMR8* in a lesser extent (Figure
141 S3). In contrast, none of the *CKIs* tested showed significant expression changes by iSPCH
142 (Figure S3), indicating that, unlike MUTE, SPCH is not a potent inducer of *CKIs*.
143 Our previous transcriptome study (Han et al., 2018) found that MUTE induces a suite
144 of cell-cycle- and mitotic division-related genes driving the SCD of stomata. To test whether
145 these genes are indeed direct MUTE targets, we performed genome-wide MUTE ChIP-
146 sequencing (see Methods) (Table S1). The overwhelming majority of MUTE-bound genes
147 (Table S2) that are upregulated by MUTE belongs to the Gene Ontology (GO) categories
148 (Table S3).: “mitotic cell cycle phase (83.22-fold enrichment, p=2.15e-02)”, “asymmetric cell
149 division (18.91-fold enrichment, p=2.4-e-02)” and other cell cycle/mitosis related categories
150 (Figure 2C, pink bars), as well as the genes involved in stomatal development: “guard mother
151 cell differentiation (37.83-fold enrichment, p=8.34e-04)” and “stomatal complex development
152 (22.7-fold enrichment, p=1.75e-12)” (Figure 2C, cyan bars). Strong MUTE-bound peaks are

153 detected at the 5'- and 3'- regions of known MUTE target loci, *ERL1, TMM, EPF2,* and
154 *CDKB1;1* (Figure 2D). Most importantly, MUTE robustly bound to the 5' region of *SMR4*,
155 indicating that *SMR4* is a direct MUTE target. As expected, no MUTE binding peak was
156 detected in *SMR1* loci, which is not induced by iMUTE and thus not a direct MUTE target
157 (Figure 2B, D).

158 We further characterized the *SMR4* expression patterns using seedlings expressing
159 nuclear-localized GFP driven by the *SMR4* promoter (Figure 2E). A strong GFP signal was
160 detected in the stomatal-lineage cells with the highest expression in a late meristemoid
161 transitioning to GMC, and persisted after SCD (Figure 2E). Likewise, a translational reporter
162 of SMR4-GFP fusion protein driven by the *SMR4* promoter exhibited similar accumulation
163 patterns predominantly in the nuclei (Figure 2F). These expression patterns mirror that of
164 MUTE (Pillitteri et al., 2007) Combined, our results indicate that MUTE directly promotes the
165 *SMR4* expression in stomatal precursor cells before the onset of the SCD. Furthermore, the
166 *SMR4* expression suggests its distinct role from canonical CKIs.

167

168 ***SMR4* suppresses cell proliferation in part with *SMR8***

169 To understand the role of *SMR4* in stomatal development, we next sought to characterize its
170 loss-of-function phenotypes. Because no T-DNA insertion line is available for *SMR4*,
171 presumably owing to its short coding sequence (219 bp), we employed CRISPR-Cas9 system
172 (Tsutsui and Higashiyama, 2017)(see Methods). A guide RNA targeting to *SMR4* yielded
173 either a base-pair deletion (*smr4-1cr*) or insertion (*smr4-2cr*) at 80 bp from the translation start
174 site, which leads to a frame shift and premature stop codon (Figure S4A, B). A quantitative
175 analysis of segmented epidermal cells (see Methods) revealed that *smr4cr* epidermis are
176 increased in small cells (< 50 μm^2) and concomitantly decreased in large pavement cells (>
177 4000 μm^2) (Figure 3A, B). Stomatal precursor cell density is also increased in *smr4cr* alleles
178 (Figure 3C). Introduction of functional *SMR4* transgene (*proSMR4::HA-SMR4*) fully rescued

179 the phenotypes of *smr4-1cr* (Figure S4D-G), indicating that increased numbers of stomata and
180 stomatal precursor cells in *smr4* are due to the loss of function of *SMR4*.
181 Because *SMR8* expression was marginally increased by iMUTE (Figure S3), we
182 further characterized the loss of function phenotypes of *SMR8.* Two T-DNA insertion lines,
183 *smr8-1* and *smr8-2,* accumulate a reduced-level of *SMR8* transcripts (Figure S4C). Like *smr4,*
184 *smr8* mutants conferred an increase in small epidermal and stomatal precursor cells, and this
185 phenotype was most exaggerated in the *smr4 smr8* double mutant (Figure 3A, B, D, E).
186 Therefore, *SMR4* plays a role in repressing ACD, including amplifying- and spacing cell
187 division of precursor cells, in part redundantly with SMR8.
188
189 **Stomatal-lineage specific expression of CKIs reveals their unique functions**
190 Our study revealed that *SMR4* is a direct MUTE target and expresses during the transition
191 from proliferating meristemoid state to differentiating GMC state. SMR proteins are known to
192 promote endoreduplication in trichomes, pavement cells and sepal giant cells (Hamdoun et
193 al., 2016; Kumar and Larkin, 2017; Roeder et al., 2010; Walker et al., 2000). However, unlike
194 trichomes and pavement cells, stomatal lineage cells do not undergo endoreduplication
195 (Melaragno et al., 1993). We thus hypothesized that SMR4 may function differently from the
196 other canonical SMRs. To address this, *SMR4, SMR8,* and *SMR1* along with *KRP1* are
197 ectopically expressed in the stomatal lineage cells (MMC, meristemoids and SLGC) by using
198 *POLAR* promoter (Pillitteri et al., 2011) (Figure 4; Figure S5). Unlike SMR1 or KRP1, *POLAR*-
199 promoter-driven SMR4 and SMR8 did not significantly changed stomatal index (number of
200 stomata /(number of stomata and non-stomatal epidermal cells) x100) (Figure 4F), reflecting
201 reduction in the number of both stomata and epidermal cells (Figure 4G, H). Whereas GMCs
202 of *POLAR*-promoter-driven SMR4 executed SCD, they formed stomata composed of skewed
203 guard cells (Figure 4B, pink bracket). This suggests that SMR4 does not inhibit the final SCD
204 *per se*. Similar deformed stomata were also observed in *proPOLAR::SMR8* (Figure 4C, pink
205 bracket).

206 Unlike SMR4, ectopic stomatal-lineage expression of SMR1 and KRP1 displayed cell
207 division defects with unique consequences. *proPOLAR::SMR1* produced abnormally large
208 undivided GMC-like cells (Figure 4D, asterisks; Figure S5), consistent with the known role of
209 SMR1 in suppressing the activity CDKB1;1 thereby promoting endoreduplication (Kumar et
210 al., 2015). Finally, *proPOLAR::KRP1* severely inhibited the ACDs, resulting in epidermis vastly
211 consisted of pavement cells with low stomatal index (Figure 4E, F), resembling with *spch*
212 mutant (MacAlister et al., 2007; Pillitteri et al., 2007).
213 The phenotype of *proPOLAR::SMR4* (and *SMR8*) is consistent with the diminished
214 proliferative activity of meristemoids. To delineate formative step from differentiation, we
215 introduced *proPOLAR::SMR4* into *mute* mutant, in which a number of amplifying ACDs are
216 increased and meristemoids arrest (Figure S5). Indeed, *proPOLAR::SMR4* significantly
217 reduced the number of ACDs, resulted in low number of larger meristemoids (Figure S5F-J).
218 Taken together, we conclude that SMR4, and some extent SMR8, possesses a unique feature
219 different from canonical CKIs to specifically terminate (but not fully inhibit) ACDs of
220 meristemoids but allows final SCD to proceed in GMC. Furthermore, formation of skewed
221 irregular-shaped stomata, some resembling pavement cells (Figure 4B), implies that
222 excessive SMR4 activity disrupt guard cell morphogenesis.
223
224 **SMR4 balances between cell proliferation and differentiation**
225 To further understand the identity of abnormally-shaped stomata observed in
226 *proPOLAR::SMR4*, stomatal lineage markers were introduced. In wild type, stomatal lineage
227 precursor marker *proTMM::GUS-GFP* (Nadeau and Sack, 2002) was detected in stomatal
228 lineage cells with the brightest signal in triangular shaped meristemoids (Figure 5A).
229 Surprisingly, both stomatal-lineage cells and enlarged pavement cell-like cells in
230 *proPOLAR::SMR4* plants expressed *proTMM::GUS-GFP* (Figure 5B). These GFP+ cells in
231 *proPOLAR::SMR4* plants sometimes divide symmetrically (Figure 5B, E, F cyan arrows).
232 Further quantitative analysis shows that, compared to wild type, these *proTMM::GUS-GFP*
233 positive cells in *proPOLAR::SMR4* are greater in size range (50~800 μm^2) and in addition

234 have low circularity (Figure 5C). This might reflect mixed cell fate; pavement cell shape with
235 stomatal identity. Some of the these cells express stomatal fate commitment marker
236 *proMUTE::nucYFP* (Figure 5F) and finally differentiate into mature guard cells (Figure 5G-I)
237 exhibiting large wavy and skewed shape (Figure 5H, I) but expressing a mature guard cell
238 marker, E994.

239 To address whether these enlarged GCs undergo endoreduplication process when
240 *SMR4* is ectopically expressed, the DNA content was measured using DAPI fluorescence.
241 Half of GC populations exhibited the fluorescence similar to the wild-type (the median value
242 is 15 μm^2 in wild type and 20 $\mu m^{2,}$ in *proPOLAR::SMR4* plants) whereas some showed
243 fluorescence values nearly doubled in *proPOLAR::SMR4* plants (Figure 5J- L). Likewise, the
244 GC nuclei size measurements using H2B-GFP (Maruyama et al., 2013) are consistent with
245 the DAPI measurements (Figure S6). The difference in nuclei size was more pronounced in
246 pavement cells. Furthermore, none of the GCs express the endoreduplication marker
247 *proSMR1::nlsGFP-GUS* (Bhosale et al., 2018) regardless of the GC size in *proPOLAR::SMR4*
248 plants, whereas pavement cells, where endoreduplication normally occurs, express GFP
249 signal (Figure 5M). Combined, these results suggest that stomatal-lineage overexprssion of
250 *SMR4* induces another round of DNA synthesis but does not trigger the endoreduplication
251 cycle in the stomatal lineage. This feature distinguishes SMR4 from the known SIM/SMR-
252 family of CKIs. The unique, non-canonical activity of SMR4 is also supported by systematic
253 stomatal-lineage overexpression of selected CKIs, where only SMR1 generated huge
254 undivided GMC cells (Figure 4D, Figure S5).

255

256 **SMR4 decelerates cell cycle progression by G1 phase extension**

257 We elucidated that stomatal-lineage ACDs are faster than the final SCD (Figure 1B, C). What
258 is the ramification of stomatal-lineage overexpression of *SMR4* on cell cycle duration of ACDs
259 and SCD? To address this question, we introduced the triple cell cycle marker PlaCCI to
260 *proPOLAR::SMR4* plants and performed time-lapse imaging (Figure 6; Movie S3). The

261 stomatal precursor cells (meristemoids) in *proPOLAR::SMR4* seedlings exhibited striking
262 extension of G1 phase (Figure 6A, from average of 3.23 to 8.03 hours), extending the total
263 cell cycle time from 12.03 to 18.47 hours (Figure 6B). In contrast, the cell cycle duration of the
264 SCD was not significantly affected by *proPOLAR::SMR4* (19.57 hours, Figure 6, Movie S4).
265 Combined, the results suggest that SMR4 can slow down cell cycle progress by G1 phase
266 extension, and that the cell cycle of proliferative ACDs, but not the final SCD, are preferentially
267 decelerated by SMR4.
268
269 **Physical and functional interactions of SMR4 with D-type cyclins underscore the swith**
270 **from ACD to SCD**
271 SIM is known to interact with CYCA2;3 to promote endoreduplication (Wang et al., 2020).
272 Unlike SIM, stomatal-lineage overexpression of *SMR4* can extend G1 cycles of ACD but
273 allows execution of the final SCD (Figures 4-6). We thus predict that SMR4 regulates the G1-
274 S transition via associating with D-type Cyclins. To understand the mode of action of SMR4,
275 we first surveyed publicly available protein-protein interactome data (Szklarczyk et al., 2019)
276 (Figure 7A). The known SMR4 interactors include major components of cell cycle progression,
277 CSK1, CKS2, CDKA;1 (CDC2), CYCD2;1, CYCD3;1 and CYCD7;1 (Figure 7A). Among them
278 CYCD3;1 is known to play a role in SPCH-mediated ACDs, and CYCD7;1 is involved in the
279 SCD of GMC (Adrian et al., 2015). Our yeast-two-hybrid (Y2H) analysis shows that consistent
280 with the interactome data (Figure 7A), SMR4 associates with CYCD3;1 and CYCD7;1. In
281 contrast, no interaction was observed for SMR4 and CYCD5;1, a direct MUTE target initiating
282 the single SCD (Han et al., 2018) (Figure 7B). We also did not observe the direct interaction
283 of SMR4 with CDKA;1 or CDKB1;1 (Figure 7B).
284 Next, to address the biological significance of SMR4 interactions with CYCD3;1 and
285 CYCD7;1 but not with CYC5;1, we examined the effects conferred by stomatal-lineage
286 overexpression of three D-type Cyclins in the presence or absence of functional *SMR4*. As
287 shown in Figure 7C and D, in the absence of *SMR4*, *POLAR*-promoter-driven expression of
288 *CYCD3;1* and *CYCD7;1* exaggerated the ACDs, resulting in significant increase in the number

289 of stomatal precursor cells. By contrast, *smr4-1cr* mutant did not affect the phenotype of
290 *proPOLAR::CYCD5;1* (Figure 7C, D). On the basis of these findings, we conclude that SRM4
291 can suppress the stomatal-lineage divisions by direct association with CYCD3;1 and CYCD7;1,
292 but not with CYCD5;1, and this differential interaction with D-type cyclins underscores the
293 transition from proliferative ACDs to final SCD (Figure 7E).
294
295
296 **Discussion**
297 In this study, we discovered that proliferative ACDs has faster cell cycle duration than the
298 single terminal SCD within the stomatal cell lineages. A subsequent genome-wide profiling of
299 MUTE targets followed by phenotypic and functional characterizations identified SMR4 as a
300 non-canonical CKI that sets a cell-cycle break to facilitate transition from ACD to SCD. SMR4
301 is a direct MUTE target specifically induced by MUTE but not by SPCH (Figure 2), thus
302 highlighting the orchestration of cell-state switch from proliferation (meristemoids) to
303 differentiation (stomata) at the control of cell cycle duration. This view is further supported by
304 the findings that prolonged G1/S phase specifically during the proliferative ACDs by stomatal-
305 lineage overexpression of *SMR4* causes mis-specification of guard cells (Figures 4, 5).
306 In contrast of SIM and SMR1, known regulators of endoreduplication (Roeder et al.,
307 2010; Wang et al., 2020), we found that SMR4 extends the G1/S transition during stomatal
308 ACDs (Figure 5). It has been shown that SIM associates with CYCA2;3 but not with CYCD3;1
309 (Wang et al., 2020). Assuming that SMR1 functions similarly to SIM, the enlarged single-celled
310 stomata conferred by the stomatal-lineage overexpression of SMR1 (Figure 4) can be
311 attributed to the direct inhibition of CYCA2;3-CDKB;1 complex by SMR1. Indeed, higher-order
312 mutations in *CYCA2s* (*cycA2;1, 2;2, 2,3* triple mutant) as well as the dominant-negative
313 inhibition of *CDKB1;1* exhibit the identical, single-celled stomata phenotypes (Boudolf et al.,
314 2004; Vanneste et al., 2011). By contrast, we found that SMR4 functionally associates with D-
315 type Cyclins (Figure 7). Thus, distinct functions among SIM/SMRs lie in their unique interaction
316 potential with different Cyclin-CDK complexes. During mammalian cell cycle, a series of CKIs

317 exhibit inhibitory roles during G1/S transition via associating with CyclinD1/2/3-CDK4/6 and
318 then with CyclinE/CDK2 complexes (Sherr and Roberts, 2004). Among them, $p27^{KIP1}$ can bind
319 with different Cyclin-CDK complexes and exert different regulatory effects on each complex
320 (Sherr and Roberts, 2004). Plants lack CyclinE, but the previous large-scale expression
321 analysis of cell cycle genes suggests that the plant CYCDs adopt both metazoan CyclinD and
322 CyclinE functions (Menges et al., 2005). That SMR4 binds with different D-type Cyclins to
323 negatively regulate G1/S phase therefore echoes its functional parallel to metazoan CKI,
324 $p27^{KIP1}$.

325 How could SMR4 decelerate cell cycles in proliferative ACDs but not in terminal SCD?
326 Our results suggest that the specificity lies on preferential association of SMR4 with different
327 CyclinDs, each with a unique expression pattern within the stomatal-cell lineages. For
328 example, *CYCD3;1* and *CYCD3;2* are induced by *SPCH* and promote ACDs (Adrian et al.,
329 2015; Han et al., 2018; Lau et al., 2014). By contrast, *CYCD5;1* is directly induced by MUTE
330 to drive the terminal SCD (Han et al., 2018). *CYCD7;1* is likely involved in the terminal SCD,
331 however, its expression starts later and persists longer than *CYCD5;1* (Han et al., 2018;
332 Weimer et al., 2018). Based on the physical and functional associations of SMR4 with
333 CYCD3;1 and CYCD7;1 but not with CYCD5;1, we propose the following model of regulatory
334 circuit driving the asymmetric-to-symmetric division switch (Figure 7E): First, SPCH initiates
335 and sustains the fast and reiterative ACDs of a meristemoid. During the meristemoid-to-GMC
336 transition, MUTE directly induces SMR4, which directly associates with CYCD3;1 (and likely
337 with CYCD3;2) and inhibit of a CYCD3;1-CKDA;1 complex to terminate amplifying ACDs. At
338 the same time, MUTE directly induces CYCD5;1. Because CYCD5;1 is not directly inhibited
339 by SMR4, the final SCD can start even in the presence of SMR4. SMR4 may fine-tune the
340 SCD by being able to inhibit the later-expressed CYCD7;1, which is likely complexed with
341 CDKA;1. The endogenous expression of SMR4 disappears immediately after the execution of
342 SCD (Figure 2F), hence the robust differentiation of stomata ensured. SMR8 has partially
343 redundant role with SMR4 and is weakly induced by both SPCH and MUTE (Figure 1) as such,
344 SMR8 is likely participating in part of this fine-tuning this transition. Unlike CycD3s and

345 CycD7;1, CycD5;1 lacks part of the core domain (Strzalka et al., 2015), which may explain the
346 differential SMR4 binding.

347 In addition to CKIs, Rb protein negatively regulates G1/S transition (Bertoli et al., 2013).
348 The plant RETINOBLASTOMA RELATED (RBR) protein functions as key cell cycle regulators
349 during stomatal development, and its reduced expression confers excessive proliferative
350 ACDs within the stomatal cell lineages, in part due to dysregulated *SPCH* expression (Borghi
351 et al., 2010; Weimer et al., 2012). Whereas both CYCD3;1 and CYCD7;1 possess LxCxE
352 RBR-binding motif, CYCD5;1 bears a variant motif, which may compromise the RBR
353 association (Vandepoele et al., 2002). Thus, CYCD5;1's unique activity to execute the single
354 SCD might involve the lack of negative regulation by RBR. Interestingly, RBR regulates the
355 expression and activities of stomatal bHLH proteins, SPCH and FAMA, respectively (Matos et
356 al., 2014; Weimer et al., 2012) but not MUTE. Thus, the commitment to differentiation by
357 MUTE-orchestrated network may be inherently resilient to inhibition at G1/S transition.

358 Our study showed that extended G1-phase by stomatal-lineage overexpression of
359 SMR4 conferred irregular-shaped meristemoids and eventual differentiation of stomata with
360 skewed guard cells. Some guard cells exhibit a jigsaw-puzzled shape, which is indicative of
361 pavement cell-like characteristics (Figures 4, 5). Thus, without timely execution of an ACD,
362 the stomatal precursor cell can adopt hybrid identity of a guard cell and pavement cell. An
363 intrinsic polarity protein BASL ensures that only one of the two daughter cells, the meristemoid,
364 maintains high SPCH levels, thereby able to reiterate proliferative ACDs (Dong et al., 2009).
365 The remaining daughter cell readily loses SPCH protein and differentiate into a pavement cell.
366 This process involves a dynamic subcellular re-localization of BASL protein between the
367 nucleus and polarly-localized cell cortex, the latter activates MAP kinase cascade that inhibits
368 SPCH protein accumulation via phosphorylation (Zhang et al., 2016; Zhang et al., 2015). It is
369 not known whether the cell cycle phase influences BASL behaviors, but our work implies that
370 could be the case.

371 The SMR4-mediated cell cycle deceleration during the meristemoid-to-GMC transition
372 mirrors the fundamental importance of G1-phase extension for cell fate decision and

373 differentiation during development (Dalton, 2015; Liu et al., 2019). The direct role of MUTE to
374 execute both termination of proliferative asymmetric divisions and orchestration of the single
375 terminal symmetric division occurs through interwoven regulation of core cell cycle drivers and
376 a braker. Understanding how cell cycle machineries in turn regulate the precise expression of
377 MUTE, which likely involves epigenetic state changes, will provide a full picture of cell cycle
378 control of cell fate specification in plants.
379
380
381 **ACKNOWLEDGEMENTS**
382 We thank Bénédicte Desvoyes and Crisanto Gutierrez for *PlaCCI*, Lieven De Veylder for
383 *proSMR1::nls-GFP*, Daisuke Kurihara for *proRPS5A::H2B-GFP*, and ABRC for GFP-Lti6B
384 and *SMR8* T-DNA lines. This work is supported by JSPS KAKENHI Grant-in-Aid for Scientific
385 Research on Innovative Areas (17H06476), WPI-ITbM operational funds, and the start-up
386 funds from the UT Austin, Molecular Biosciences to KUT. KUT acknowledges the support from
387 Howard Hughes Medical Institute and Johnson & Johnson Centennial Chair of Plant Cell
388 Biology at the UT Austin. SKH was supported by the Young Leader Cultivation Program from
389 the Institute of Advanced Research, Nagoya University.
390
391
392 **AUTHOR CONTRIBUTIONS**
393 Conceptualization, S.-K.H. and K.U.T.; Experimental Design, S.-K.H, E.-D.K. and K.U.T.;
394 Performance of experiments, S.-K.H., J.Y., M.A., R.I., T.S.; Bioinformatics Analysis, S.-K.H.,
395 S.K., E.-D.K. and K.U.T.; Visualization, S.-K.H., J.Y., K.U.T; Writing- Original Draft, S.-K.H.
396 and K.U.T.; Writing- Review & Editing, S.-K.H., J.Y., E.-D.K., K.U.T; Project Administration,
397 K.U.T.; Funding Acquisition, K.U.T.
398
399

400 **MATERIALS AND METHODS**

401

402 **Plasmid Construction and Plant materials**

403 For a detailed information of constructs generated in this study, see Table S4. Primers used
404 for plasmid constructs were listed in Table S5-7. For generation of transgenic Arabidopsis,
405 plasmid constructs were electroporated into Agrobacterium (GV3101/pMP90) and
406 subsequently transformed by floral dipping. Loss-of-function mutant of *SMR4* was generated
407 by CRISPR by using pKAMA-ITACHI Vector (Addgene: 85808) as described previously
408 (Tsutsui and Higashiyama, 2017). Briefly, primers for sgRNA were designed by the CCTop -
409 CRISPR/Cas9 target online predictor (Stemmer et al., 2015). Primers were annealed and
410 inserted into pKI1.1R vector cut with *AarI*. Resulting construct was introduced into wild-type
411 Col-0 plants. T1 plants were screened by Hygromycin resistance. Six T1 lines were selected
412 and sequenced to check whether mutations were introduced. One of the two sgRNAs was
413 successful for generating mutations. In T2 generation, seeds that do not show OLE1-RFP
414 signal were selected to exclude plants harboring transgene in the genome. We established
415 two independent homozygous lines that contain 1 bp deletion (*smr4-1*) or 1 bp insertion *(smr4-*
416 *2)* at *SMR4* gene (Figure S4). Primers used single guide RNA (sgRNA) for *SMR4* were listed
417 in Table S6. T-DNA insertion mutants of *SMR8, smr8-1* (SALK_126253), *smr8-2*
418 (SALK_074523) were obtained from ABRC. Their genotype and transcript reduction were
419 confirmed. Genotyping- and qRT-PCR primers were listed in Table S7. All plant materials used
420 in this study were listed in Key Resource Table.

421

422 **Plant growth condition and estradiol treatment**

423 Arabidopsis accession Columbia (Col-0) was used as wild-type. Sterilized seeds were grown
424 on half strength of Murashige and Skoog (MS) media with 1% sucrose at 22°C under
425 continuous light. 10~14-day-old seedlings grown on MS media were transplanted to soil. For
426 phenotyping of transgenic plants, either T1 or T2 plants were grown on ½ MS agar media
427 containing hygromycin (20 μg/ml). For the complementation test of SMR4, T3 homozygous

428 plants of *proSMR4::HA-SMR4* were germinated on ½ MS agar media with 1% sucrose and
429 were imaged at 5-day post germination (dpg).
430
431 **Confocal microscopy**
432 For confocal microscopy, cell peripheries of seedlings were visualized with either propidium
433 iodide (Sigma, P4170) or FM4-64 (Invitrogen, T13320). Images were acquired using LSM800
434 (Zeiss) or SP5-WLL (Leica) using a 63x water lens. The Zeiss LSM800 was used to image the
435 GFP and RFP reporter with excitation at 488 nm and an emission filter of 490 to 546 nm, and
436 with excitation at 555 nm and 583-617 nm emission range, respectively. PlaCCI lines
437 (Desvoyes et al., 2020) were imaged using SP5-WLL with the following conditions: CFP,
438 excitation at 458 nm and emission from 468 to 600 nm; GFP, excitation at 488 nm and
439 emission from 490 to 546 nm; YFP, excitation at 514 nm and emission from 524 to 650 nm;
440 mCherry, excitation at 560 nm and emission from 590 to 650 nm. Signals were visualized
441 sequentially using separate HyD detectors. DIC images were taken to delineate the cell
442 outlines (shown in magenta). Raw data were collected with 1024 x 1024 pixel image and
443 imported into Fiji-ImageJ to generate CYMK images using the channel merge function. The
444 time-lapse were collected at 30-min intervals using a 20x lens (Peterson and Torii, 2012; Qi
445 et al., 2017). Raw images were imported into Fiji-ImageJ to generate time projections using
446 the Stacks function.
447
448 **Quantitative analysis of epidermal phenotype**
449 For quantitative analysis of leaf epidermis of *smr* mutants, confocal images were taken at 4
450 days after germination. Preparation of images was done as described previously (Houbaert et
451 al., 2018). For counting epidermal cell types, the number of stomata, number of stomatal
452 lineage precursors (meristemoids and GMC), total epidermal cells (stomata, meristemoids,
453 GMC and pavement cells) and stomata index (number of stomata / number of total epidermal
454 cells x100) were calculated by counting cell types in an area of 0.45 mm^2 (0.67 mm x 0.67
455 mm) at the developmental stage indicated with the cell counter plug-in in Fiji. The epidermal

456 cell areas of *smr* mutants were color-coded depending on the area calculated using
457 ROI_Color_Coder with a range of min-max (0-4000) in Fiji. The epidermal cells were
458 subdivided into 9 groups according to their size. One representative image from each
459 genotype was analyzed and the cell size distribution was then calculated from 499 cells for
460 Col-0 plants, 659 cells for *smr4-1*, 662 cells for *smr4-2*, 601 cells form *smr8-1*, 611 cells form
461 *smr8-1* and 755 cells for *smr4-1 smr8-1* double mutant. Guard cells were excluded for the cell
462 size measurement.

463 For cell size and circularity measurement of stomatal lineage precursors, images of
464 *proTMM::GUS-GFP* were set to grayscale and GFP expressing cells were colored in black
465 while other cell area in white by photoshop, then the images were imported to Fiji. Imported
466 images were subjected to Images > Threshold; Analyze > analyze particle. Shape descriptors
467 box has to be checked in "Set measurement" under the Analyze tab to get circularity values
468 from the selected cell area. For the meristemoid size in *mute* mutant background was
469 measured by the same methods.

470

471 **cDNA preparation and qRT-PCR**

472 For chemical treatment, plants were grown on media containing either 10uM β-estradiol
473 (Sigma, E8875) or DMSO. For time-course induction, estradiol-inducible MUTE or SPCH
474 seeds were sown on 1/2 MS media, and subjected to stratification at 4°C for two to three days
475 then grown for the four to five days under continuous light. Subsequent steps were performed
476 as described Han et al., 2018 (Han et al., 2018). RNA was isolated using RNeasey Plant Mini
477 Kit (Qiagen, 74904). 0.5 µg of RNA was converted to cDNA using ReverTra Ace™ qPCR RT
478 Master Mix with gDNA Remover (TOYOBO, FSQ-301) according to the instructions of the
479 manufacturer. qRT-PCR was performed as described in Han et al., 2018 (Han et al., 2018)
480 using KAPA SYBR® FAST qPCR Kit Master Mix on LightCycler® 96 instrument (Roche).
481 Relative expression was calculated by dividing *ACTIN2* gene expression over the specific-
482 gene expression and the fold change was calculated by dividing estradiol expression over

483 DMSO (mock) expression at each time point indicated. See Table S7 for primer sequences
484 used for qRT-PCR.
485
486 **Chromatin Immunoprecipitation Sequencing (ChIP-seq)**
487 For MUTE ChIP-seq experiments, transgenic plants *proMUTE::MUTE-GFP scrm-D* were
488 prepared as described previously (Han et al., 2018) with following modifications. To shear the
489 DNA, Bioruptor (Diagnode) was used, 30 sec on and 30 sec off cycle 15~18 times.
490 Immunoprecipitation against GFP was performed using anti-GFP antibody (Abcam, ab290,
491 Lot. GR318425-1). DNAs from the immuno-complex was purified by kit (Zymo Research,
492 D5205). The half of the purified DNA was subjected to library preparation using ACCEL-NGS®
493 2S PLUS DNA LIBRARY KIT with 2S Set A MID Indexing Kit (Swift bioscience, 21024, 26148)
494 for next generation sequencing. Quantitative PCR (qPCR) was carried out using gene specific
495 primers (Table S7) to confirm the library construction. The qPCR was run using KAPA SYBR®
496 FAST qPCR Kit Master Mix on LightCycler® 96 instrument (Roche) as described previously
497 described (Han *et al*., 2018). Three biological replicates were used for MUTE ChIP-seq
498 experiments. Size distribution of the libraries was validated by 2100 Bioanalyzer (Agilent). The
499 prepared libraries (Col input and IP, MUTE-GFP input and IP with three replicates) were
500 sequenced 35 bp paired-end in length with 30million coverage per sample on Illumina
501 NextSeq 500 system. ChIP mapping and peak calling were performed as described in Feng
502 et al., 2012 (Feng et al., 2012). Output reads were mapped to the TAIR10 genome assembly
503 using bowtie2 and resulting bam files were sorted and indexed via samtool. The sorted bam
504 files were subjected for MACS peak calling (version 2.1.0.20140616) (Table S2). Bedgraph
505 file was generated and visualized in igv browser. Gene Ontology enrichment analysis was
506 performed using GENE ONTOLOGY (http://geneontology.org/) combined with manual
507 curation to remove redundant terms. Genes increased by MUTE more than Log2 FC 0.4 and
508 targeted by MUTE were tested. Following multiple hypothesis testing correction (Bonferroni-
509 correction), GO term with FDR <0.05 were called significantly enriched (Table S3). The ChIP-

510 seq data generated in this study are deposited to the NCBI Gene Expression Omnibus (GEO)
511 with an accession number GEO: GSE173338.
512
513 **Measurement of DNA content and nuclei size**
514 1st true leaves were harvested from 16 day old plants and fixed in a solution of 9:1 (v/v)
515 ethanol:acetic acid for overnight. For DAPI staining, tissues were rehydrated with ethanol
516 series. DAPI (4'6-diamidino-2'-phenylindole) staining was done in 5µg/ml final concentration
517 for 15 minutes in dark. Nuclear DAPI fluorescence was excited at 405nm captured with 410 -
518 470 nm emission range. DAPI stained nuclei area from the guard cells was selected and
519 measured by using FIJI software. Wild-type and two independent T2 *proPOLAR::SMR4*
520 transgenic lines were used. number of guard cells measured, 129 (WT) and 234
521 (*proPOLAR::SMR4*). 10 or 11-day-old cotyledons from *proRPS5A::H2B* (Maruyama et al.,
522 2013) transgenic plants were also imaged to measure the nuclei size of guard- and pavement
523 cells. The area of nuclei (GFP) was selected and measured from the z-stack projection images
524 using FIJI software. Number of guard cells and pavement cells measured, 155 and 108 (wild
525 type); 191 and 103 (*proPOLAR::SMR4 proRPS5A::H2B*).
526
527 **Yeast two hybrid assay**
528 Y2H assays were performed using the Matchmaker^{TM} Two-Hybrid System (Clontech). Bait
529 (pGBKT7) and prey (pGADT7) constructs were co-transformed into the yeast strain AH109
530 according to manufactural instruction (Clontech). The resulting transformants were spotted on
531 SD (−Leu, −Trp) and SD (−Trp, −Leu, −His) selection media containing different concentration
532 of 3-amino-1,2,4-triazole (Sigma, A8056) as previously reported (Putarjunan et al., 2019). All
533 constructs and primer information are listed in the Tables S4 and S5.
534
535
536

537 **REFERENCES**
538
539 Adrian, J., Chang, J., Ballenger, C.E., Bargmann, B.O., Alassimone, J., Davies, K.A., Lau,
540 O.S., Matos, J.L., Hachez, C., Lanctot, A.*, et al.* (2015). Transcriptome dynamics of the
541 stomatal lineage: birth, amplification, and termination of a self-renewing population. Dev Cell
542 *33*, 107-118.
543 Bertoli, C., Skotheim, J.M., and de Bruin, R.A. (2013). Control of cell cycle transcription
544 during G1 and S phases. Nat Rev Mol Cell Biol *14*, 518-528.
545 Bhosale, R., Boudolf, V., Cuevas, F., Lu, R., Eekhout, T., Hu, Z., Van Isterdael, G., Lambert,
546 G.M., Xu, F., Nowack, M.K.*, et al.* (2018). A Spatiotemporal DNA Endoploidy Map of the
547 Arabidopsis Root Reveals Roles for the Endocycle in Root Development and Stress
548 Adaptation. Plant Cell *30*, 2330-2351.
549 Borghi, L., Gutzat, R., Futterer, J., Laizet, Y., Hennig, L., and Gruissem, W. (2010).
550 Arabidopsis RETINOBLASTOMA-RELATED is required for stem cell maintenance, cell
551 differentiation, and lateral organ production. Plant Cell *22*, 1792-1811.
552 Boudolf, V., Barroco, R., Engler Jde, A., Verkest, A., Beeckman, T., Naudts, M., Inze, D.,
553 and De Veylder, L. (2004). B1-type cyclin-dependent kinases are essential for the formation
554 of stomatal complexes in Arabidopsis thaliana. Plant Cell *16*, 945-955.
555 Budirahardja, Y., and Gonczy, P. (2009). Coupling the cell cycle to development.
556 Development *136*, 2861-2872.
557 Coronado, D., Godet, M., Bourillot, P.Y., Tapponnier, Y., Bernat, A., Petit, M., Afanassieff,
558 M., Markossian, S., Malashicheva, A., Iacone, R.*, et al.* (2013). A short G1 phase is an
559 intrinsic determinant of naive embryonic stem cell pluripotency. Stem Cell Res *10*, 118-131.
560 Dalton, S. (2015). Linking the Cell Cycle to Cell Fate Decisions. Trends Cell Biol *25*, 592-
561 600.
562 Desvoyes, B., Arana-Echarri, A., Barea, M.D., and Gutierrez, C. (2020). A comprehensive
563 fluorescent sensor for spatiotemporal cell cycle analysis in Arabidopsis. Nat Plants *6*, 1330-
564 1334.
565 Dong, J., MacAlister, C.A., and Bergmann, D.C. (2009). BASL controls asymmetric cell
566 division in Arabidopsis. Cell *137*, 1320-1330.
567 Elledge, S.J. (1996). Cell cycle checkpoints: preventing an identity crisis. Science *274*, 1664-
568 1672.
569 Feng, J., Liu, T., Qin, B., Zhang, Y., and Liu, X.S. (2012). Identifying ChIP-seq enrichment
570 using MACS. Nat Protoc *7*, 1728-1740.
571 Hachez, C., Ohashi-Ito, K., Dong, J., and Bergmann, D.C. (2011). Differentiation of
572 Arabidopsis guard cells: analysis of the networks incorporating the basic helix-loop-helix
573 transcription factor, FAMA. Plant Physiol *155*, 1458-1472.
574 Hamdoun, S., Zhang, C., Gill, M., Kumar, N., Churchman, M., Larkin, J.C., Kwon, A., and Lu,
575 H. (2016). Differential Roles of Two Homologous Cyclin-Dependent Kinase Inhibitor Genes
576 in Regulating Cell Cycle and Innate Immunity in Arabidopsis. Plant Physiol *170*, 515-527.
577 Han, S.K., Qi, X., Sugihara, K., Dang, J.H., Endo, T.A., Miller, K.L., Kim, E.D., Miura, T., and
578 Torii, K.U. (2018). MUTE Directly Orchestrates Cell-State Switch and the Single Symmetric
579 Division to Create Stomata. Dev Cell *45*, 303-315.e305.
580 Han, S.K., and Torii, K.U. (2016). Lineage-specific stem cells, signals and asymmetries
581 during stomatal development. Development *143*, 1259-1270.
582 Harashima, H., Dissmeyer, N., and Schnittger, A. (2013). Cell cycle control across the
583 eukaryotic kingdom. Trends Cell Biol *23*, 345-356.
584 Houbaert, A., Zhang, C., Tiwari, M., Wang, K., de Marcos Serrano, A., Savatin, D.V., Urs,
585 M.J., Zhiponova, M.K., Gudesblat, G.E., Vanhoutte, I.*, et al.* (2018). POLAR-guided
586 signalling complex assembly and localization drive asymmetric cell division. Nature *563*,
587 574-578.
588 Inze, D., and De Veylder, L. (2006). Cell cycle regulation in plant development. Annu Rev
589 Genet *40*, 77-105.
590 Kumar, N., Harashima, H., Kalve, S., Bramsiepe, J., Wang, K., Sizani, B.L., Bertrand, L.L.,
591 Johnson, M.C., Faulk, C., Dale, R.*, et al.* (2015). Functional Conservation in the SIAMESE-

592 RELATED Family of Cyclin-Dependent Kinase Inhibitors in Land Plants. Plant Cell *27*, 3065-
593 3080.
594 Kumar, N., and Larkin, J.C. (2017). Why do plants need so many cyclin-dependent kinase
595 inhibitors? Plant Signal Behav *12*, e1282021.
596 Lau, O.S., and Bergmann, D.C. (2012). Stomatal development: a plant's perspective on cell
597 polarity, cell fate transitions and intercellular communication. Development *139*, 3683-3692.
598 Lau, O.S., Davies, K.A., Chang, J., Adrian, J., Rowe, M.H., Ballenger, C.E., and Bergmann,
599 D.C. (2014). Direct roles of SPEECHLESS in the specification of stomatal self-renewing
600 cells. Science *345*, 1605-1609.
601 Liu, L., Michowski, W., Kolodziejczyk, A., and Sicinski, P. (2019). The cell cycle in stem cell
602 proliferation, pluripotency and differentiation. Nat Cell Biol *21*, 1060-1067.
603 MacAlister, C.A., Ohashi-Ito, K., and Bergmann, D.C. (2007). Transcription factor control of
604 asymmetric cell divisions that establish the stomatal lineage. Nature *445*, 537-540.
605 Maruyama, D., Hamamura, Y., Takeuchi, H., Susaki, D., Nishimaki, M., Kurihara, D.,
606 Kasahara, R.D., and Higashiyama, T. (2013). Independent control by each female gamete
607 prevents the attraction of multiple pollen tubes. Dev Cell *25*, 317-323.
608 Matos, J.L., Lau, O.S., Hachez, C., Cruz-Ramirez, A., Scheres, B., and Bergmann, D.C.
609 (2014). Irreversible fate commitment in the Arabidopsis stomatal lineage requires a FAMA
610 and RETINOBLASTOMA-RELATED module. Elife *3*.
611 Melaragno, J.E., Mehrotra, B., and Coleman, A.W. (1993). Relationship between
612 Endopolyploidy and Cell Size in Epidermal Tissue of Arabidopsis. Plant Cell *5*, 1661-1668.
613 Menges, M., de Jager, S.M., Gruissem, W., and Murray, J.A. (2005). Global analysis of the
614 core cell cycle regulators of Arabidopsis identifies novel genes, reveals multiple and highly
615 specific profiles of expression and provides a coherent model for plant cell cycle control.
616 Plant J *41*, 546-566.
617 Morgan, D.O. (2007). The cell cycle : principles of control (London: New Science Press Ltd
618 in association with Oxford University Press).
619 Nadeau, J.A., and Sack, F.D. (2002). Control of stomatal distribution on the Arabidopsis leaf
620 surface. Science *296*, 1697-1700.
621 Peres, A., Churchman, M.L., Hariharan, S., Himanen, K., Verkest, A., Vandepoele, K.,
622 Magyar, Z., Hatzfeld, Y., Van Der Schueren, E., Beemster, G.T.*, et al.* (2007). Novel plant-
623 specific cyclin-dependent kinase inhibitors induced by biotic and abiotic stresses. J Biol
624 Chem *282*, 25588-25596.
625 Peterson, K.M., and Torii, K.U. (2012). Long-term, high-resolution confocal time lapse
626 imaging of Arabidopsis cotyledon epidermis during germination. J Vis Exp.
627 Pillitteri, L.J., Peterson, K.M., Horst, R.J., and Torii, K.U. (2011). Molecular profiling of
628 stomatal meristemoids reveals new component of asymmetric cell division and
629 commonalities among stem cell populations in Arabidopsis. Plant Cell *23*, 3260-3275.
630 Pillitteri, L.J., Sloan, D.B., Bogenschutz, N.L., and Torii, K.U. (2007). Termination of
631 asymmetric cell division and differentiation of stomata. Nature *445*, 501-505.
632 Putarjunan, A., Ruble, J., Srivastava, A., Zhao, C., Rychel, A.L., Hofstetter, A.K., Tang, X.,
633 Zhu, J.K., Tama, F., Zheng, N.*, et al.* (2019). Bipartite anchoring of SCREAM enforces
634 stomatal initiation by coupling MAP kinases to SPEECHLESS. Nat Plants *5*, 742-754.
635 Qi, X., Han, S.K., Dang, J.H., Garrick, J.M., Ito, M., Hofstetter, A.K., and Torii, K.U. (2017).
636 Autocrine regulation of stomatal differentiation potential by EPF1 and ERECTA-LIKE1
637 ligand-receptor signaling. Elife *6*.
638 Roeder, A.H., Chickarmane, V., Cunha, A., Obara, B., Manjunath, B.S., and Meyerowitz,
639 E.M. (2010). Variability in the control of cell division underlies sepal epidermal patterning in
640 Arabidopsis thaliana. PLoS Biol *8*, e1000367.
641 Sanz, L., Dewitte, W., Forzani, C., Patell, F., Nieuwland, J., Wen, B., Quelhas, P., De Jager,
642 S., Titmus, C., Campilho, A.*, et al.* (2011). The Arabidopsis D-type cyclin CYCD2;1 and the
643 inhibitor ICK2/KRP2 modulate auxin-induced lateral root formation. Plant Cell *23*, 641-660.
644 Sherr, C.J., and Roberts, J.M. (2004). Living with or without cyclins and cyclin-dependent
645 kinases. Genes Dev *18*, 2699-2711.

646 Sozzani, R., Cui, H., Moreno-Risueno, M.A., Busch, W., Van Norman, J.M., Vernoux, T.,
647 Brady, S.M., Dewitte, W., Murray, J.A., and Benfey, P.N. (2010). Spatiotemporal regulation
648 of cell-cycle genes by SHORTROOT links patterning and growth. Nature *466*, 128-132.
649 Stemmer, M., Thumberger, T., Del Sol Keyer, M., Wittbrodt, J., and Mateo, J.L. (2015).
650 CCTop: An Intuitive, Flexible and Reliable CRISPR/Cas9 Target Prediction Tool. PLoS One
651 *10*, e0124633.
652 Strzalka, W.K., Aggarwal, C., Krzeszowiec, W., Jakubowska, A., Sztatelman, O., and Banas,
653 A.K. (2015). Arabidopsis PCNAs form complexes with selected D-type cyclins. Front Plant
654 Sci *6*, 516.
655 Szklarczyk, D., Gable, A.L., Lyon, D., Junge, A., Wyder, S., Huerta-Cepas, J., Simonovic,
656 M., Doncheva, N.T., Morris, J.H., Bork, P.*, et al.* (2019). STRING v11: protein-protein
657 association networks with increased coverage, supporting functional discovery in genome-
658 wide experimental datasets. Nucleic Acids Res *47*, D607-D613.
659 Tsutsui, H., and Higashiyama, T. (2017). pKAMA-ITACHI Vectors for Highly Efficient
660 CRISPR/Cas9-Mediated Gene Knockout in Arabidopsis thaliana. Plant Cell Physiol *58*, 46-
661 56.
662 Vandepoele, K., Raes, J., De Veylder, L., Rouze, P., Rombauts, S., and Inze, D. (2002).
663 Genome-wide analysis of core cell cycle genes in Arabidopsis. Plant Cell *14*, 903-916.
664 Vanneste, S., Coppens, F., Lee, E., Donner, T.J., Xie, Z., Van Isterdael, G., Dhondt, S., De
665 Winter, F., De Rybel, B., Vuylsteke, M.*, et al.* (2011). Developmental regulation of CYCA2s
666 contributes to tissue-specific proliferation in Arabidopsis. EMBO J *30*, 3430-3441.
667 Vaten, A., Soyars, C.L., Tarr, P.T., Nimchuk, Z.L., and Bergmann, D.C. (2018). Modulation
668 of Asymmetric Division Diversity through Cytokinin and SPEECHLESS Regulatory
669 Interactions in the Arabidopsis Stomatal Lineage. Dev Cell *47*, 53-66 e55.
670 Walker, J.D., Oppenheimer, D.G., Concienne, J., and Larkin, J.C. (2000). SIAMESE, a gene
671 controlling the endoreduplication cell cycle in Arabidopsis thaliana trichomes. Development
672 *127*, 3931-3940.
673 Wang, K., Ndathe, R.W., Kumar, N., Zeringue, E.A., Kato, N., and Larkin, J.C. (2020). The
674 CDK Inhibitor SIAMESE Targets Both CDKA;1 and CDKB1 Complexes to Establish
675 Endoreplication in Trichomes. Plant Physiol *184*, 165-175.
676 Weimer, A.K., Matos, J.L., Sharma, N., Patell, F., Murray, J.A.H., Dewitte, W., and
677 Bergmann, D.C. (2018). Lineage- and stage-specific expressed CYCD7;1 coordinates the
678 single symmetric division that creates stomatal guard cells. Development *145*.
679 Weimer, A.K., Nowack, M.K., Bouyer, D., Zhao, X., Harashima, H., Naseer, S., De Winter,
680 F., Dissmeyer, N., Geldner, N., and Schnittger, A. (2012). Retinoblastoma related1 regulates
681 asymmetric cell divisions in Arabidopsis. Plant Cell *24*, 4083-4095.
682 Xie, Z., Lee, E., Lucas, J.R., Morohashi, K., Li, D., Murray, J.A., Sack, F.D., and Grotewold,
683 E. (2010). Regulation of cell proliferation in the stomatal lineage by the Arabidopsis MYB
684 FOUR LIPS via direct targeting of core cell cycle genes. Plant Cell *22*, 2306-2321.
685 Zhang, Y., Guo, X., and Dong, J. (2016). Phosphorylation of the Polarity Protein BASL
686 Differentiates Asymmetric Cell Fate through MAPKs and SPCH. Curr Biol *26*, 2957-2965.
687 Zhang, Y., Wang, P., Shao, W., Zhu, J.K., and Dong, J. (2015). The BASL polarity protein
688 controls a MAPK signaling feedback loop in asymmetric cell division. Dev Cell *33*, 136-149.
689

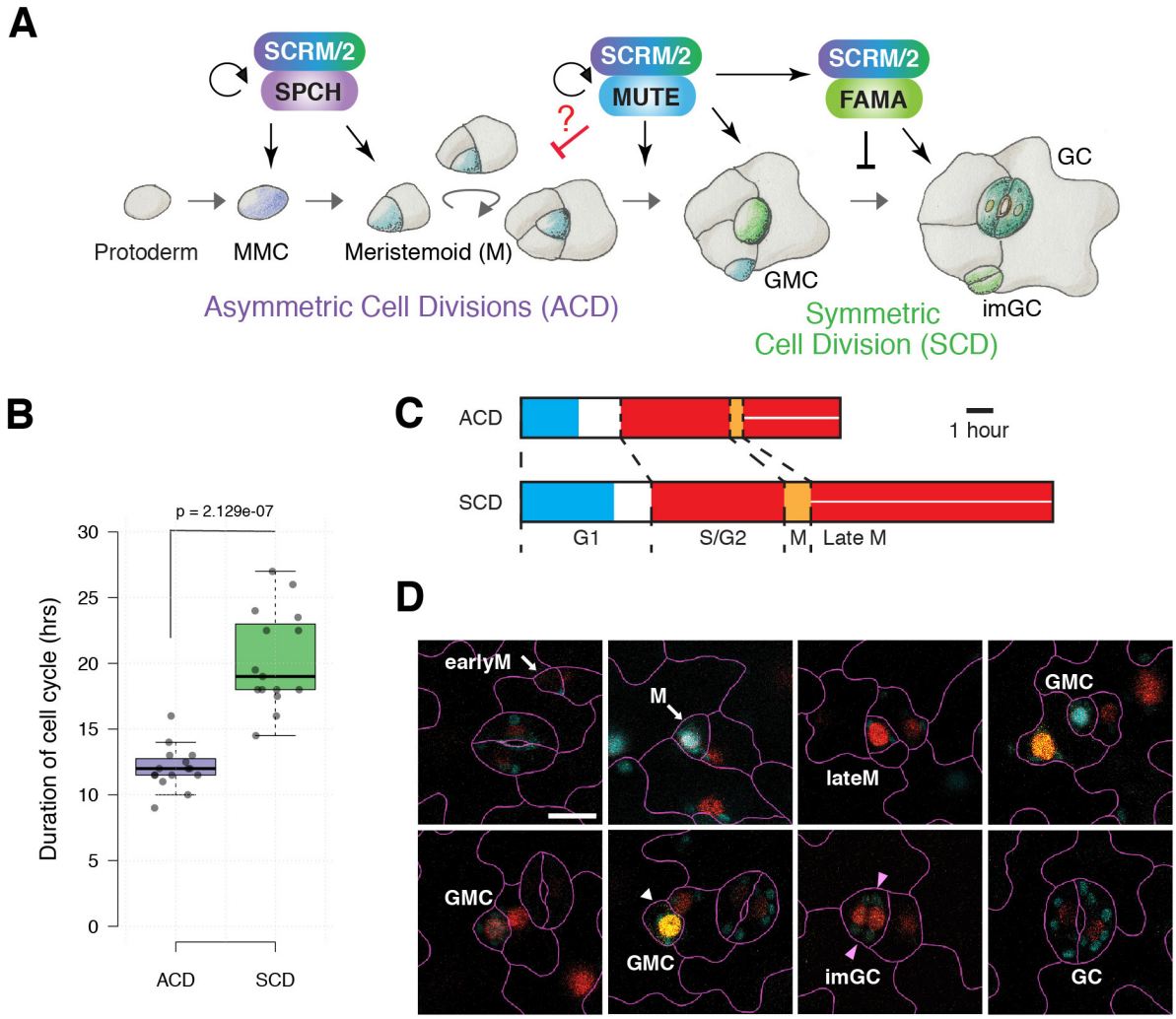

Figure 1. Cell cycle duration between asymmetric cell division and symmetric cell division during stomatal development.

(A) Cartoon to show the key heterodimeric transcription factors for each state of stomatal development, which is accompanied by a series of asymmetric cell division (ACD) triggered by SPCH·SCRM/2 and single round of symmetric cell division (SCD) coordinated by MUTE·SCRM/2 and FAMA·SCRM/2. The molecular detail how the mode of cell cycle from ACD to SCD by MUTE·SCRM/2 has not been elucidated (red line and question mark in red). MMC: meristemoid mother cell, GMC: guard mother cell, GC: guard cell.

(B) Duration of the cell cycle time of stomatal precursors undergoing ACD and SCD. n=15 for each cell division mode. Two-tailed Student t-test was performed. $p=2.129e^{-07}$.

(C) Duration of each cell cycle phase calculated from fluorescence intensity of each marker in PlaCC1. CDT1a-CFP signal (cyan) appears at the onset of G1 phase. HTR13-mCherry signal (red) accumulates when cells enter S phase and continues to late M phase. CYCB1;1-YFP signal (orange) increases in early M phase and later two separated red nuclei indicate the post division events (red with a line). Arrow: MMC; Arrowhead: GMC. Scale bar: 1 hour

(D) Confocal images of stomatal lineage cells from 4-day-old cotyledon of Col-0 expressing three PlaCCI markers. M: Meristemoid; GMC: Guard mother cell; imGC: immature GC; GC: Guard cells. Scale bar: 10 μm

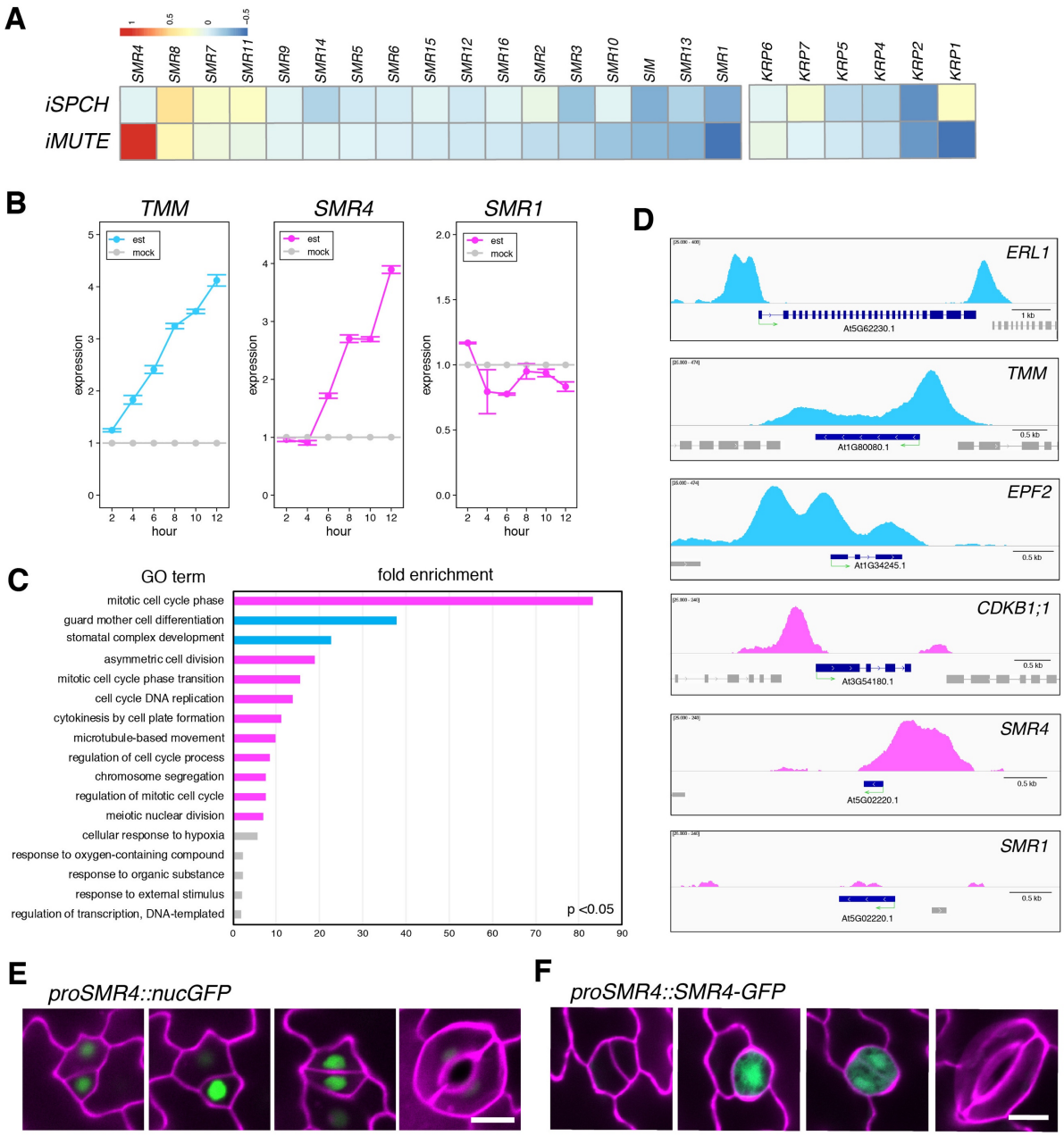

Figure 2. SMR4, one of the plant specific CKIs, expresses in stomatal lineage and is a direct target of MUTE.

(A) Heat map represents the changes in expression of 24 CKIs in Arabidopsis by SPCH or MUTE induction. RNA-seq data adopted from Lau et al., 2014 (Lau et al., 2014) (*iSPCH*) and Han et al., 2018 (Han et al., 2018) (*iMUTE*). Heat map denotes $\log_2$ ratio of changes in expression compared to non-induced control. (B) Time course expression for 12 hours with 2-hour-interval of SMRs by iMUTE monitored by qRT-PCR. TMM used as a positive control as a MUTE inducible gene. est: 10 μM estradiol treated, mock: non-treated control (DMSO only). (C) GO categories of direct MUTE targets (MUTE bound, iMUTE up) ranked by fold enrichment compared to background genome. P< 0.05. Pink bars: "cell cycle", "division", "mitotic" categories, Blue bars: "stomatal" categories, Grey bars: others

(D) IGV snapshots of ChIP-seq profile of MUTE binding to the promoter SMR4 and known MUTE targets (ERL1, TMM, EPF2, CDKB1;1) (Han et al., 2018; Qi et al., 2017). no MUTE binding was detected to *SMR1* loci. Green arrow under the gene annotation indicates gene orientation and transcriptional start sites.

(E, F) Expression patterns of *SMR4* transcriptional and translational reporters. *proSMR4::nls-3xGFP* (E) and *proSMR4::SMR4-GFP* (F) in stomatal lineage precursor cell specific on the epidermis. Scale bar, 20 μm

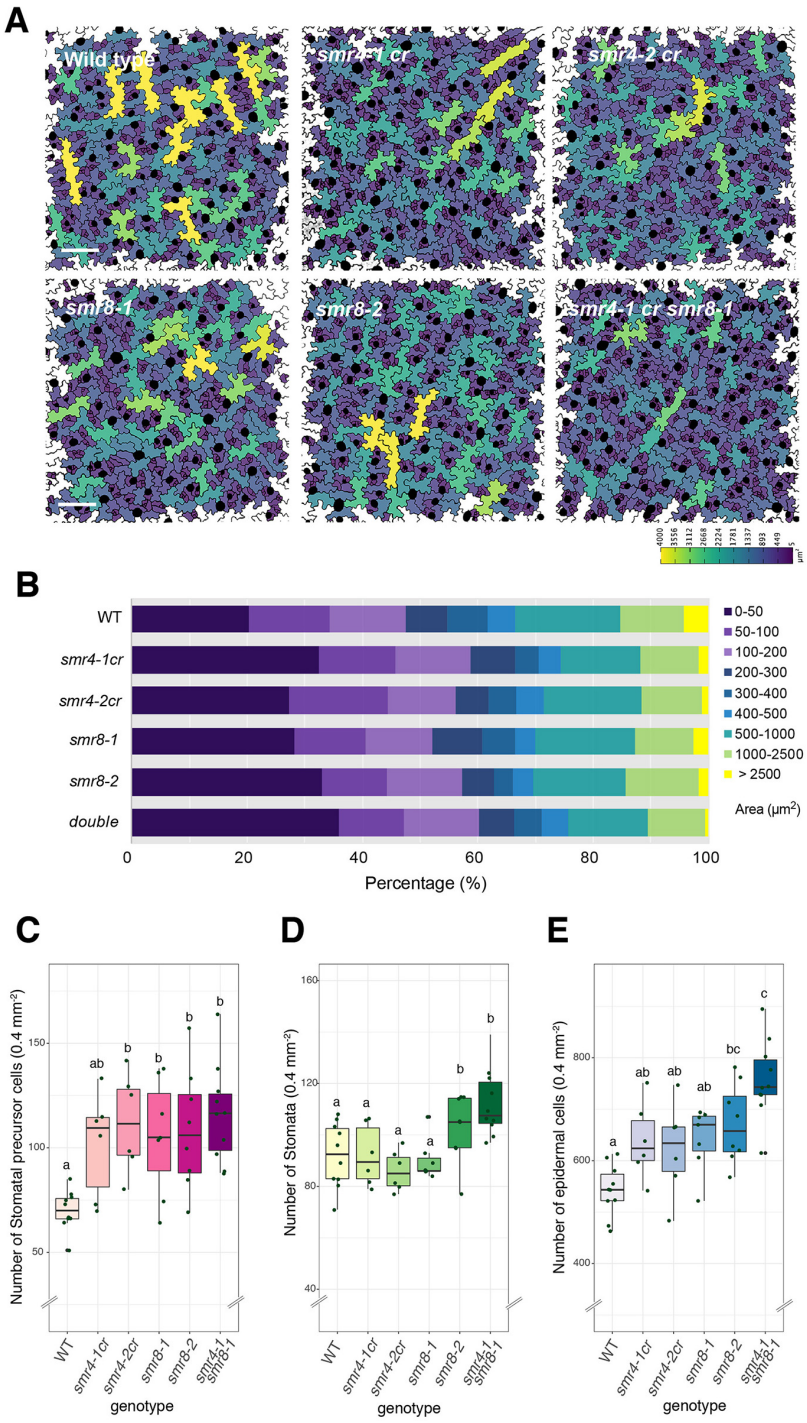

Figure 3. *smr4* CRISPR knockout mutants produce smaller cells, the phenotype enhanced by *smr8*

(A) Abaxial epidermis of cotyledons at 4-day-old seedlings of wild-type, *smr4-1cr*, *smr4-2*cr *smr8-1* and *smr4-1 smr8-1* double mutant Arabidopsis plants. Epidermal cells size is color-coded as a color scale at bottom. Scale bar, 100 μm

(B) Bar graphs showing the percentage of each category of cell area from the images for the genotype presented in (A).

(C-E) Quantification data of the number of stomatal precursor cells (meristemoid + GMC) (C), stomata (D), and total epidermal cells (E) per 0.4mm^{-2} area for the genotypes shown in (A). One-way ANOVA followed by Tukey's post hoc test was performed for comparing all genotypes. Different letter denotes significant difference. Double letter denotes insignificance. P <0.05 or P<0.01. The number of plants from each genotype, WT: n=10, *smr4-1cr*: n=6, *smr4-2cr*: n=6, *smr8-1*: n=7 , *smr8-2*: n= 8, *smr8-1 smr8-2*: n=10

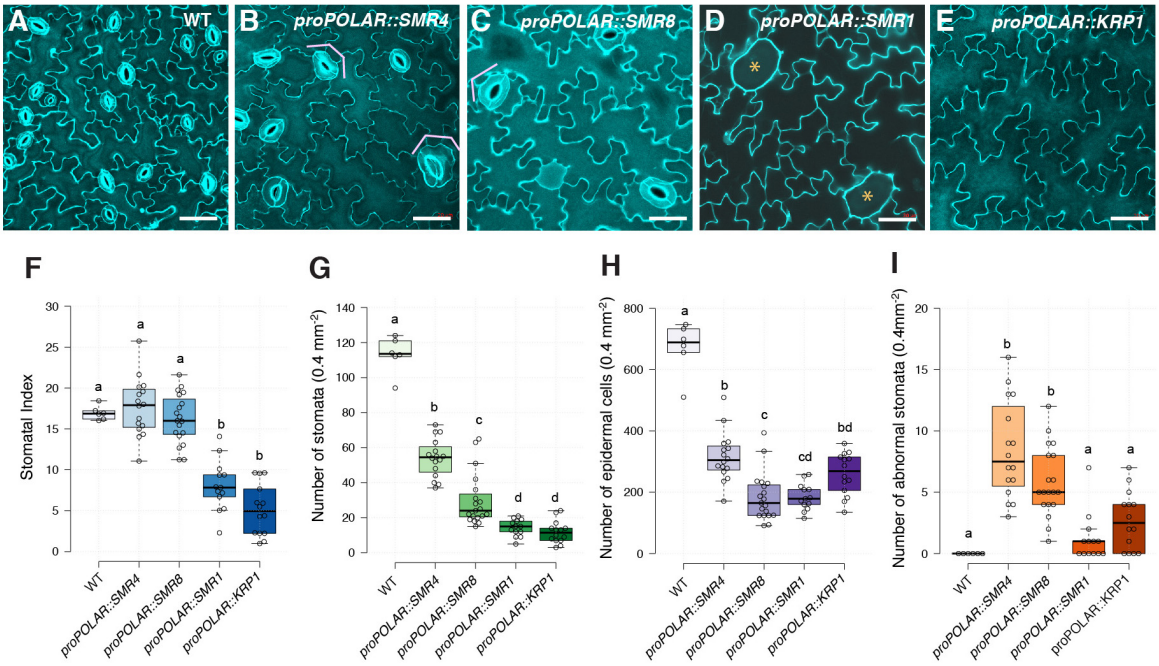

Figure 4. Stomatal-lineage overexpression phenotype of a suite of CKIs reveal their unique activities

(A-E) Epidermal phenotype of abaxial cotyledon in 8-day old wild type (WT: A), *proPOLAR::SMR4* (B), *proPOLAR::SMR8* (C), *proPOLAR::SMR1* (D), *proPOLAR::KRP1* (E). Scale bar, 50 µm; Orange asterisks, undivided single-celled stomata

(F-I) Quantification of epidermal cell number of abaxial cotyledon in 4-day old WT and transgenic plants. Stomatal Index (F) as well as number of stomata (G) number of epidermal cells (H), and number of abnormal stomata (I) in 0.4mm^{-2} area. One-way ANOVA with Tukey's post hoc test was performed to compare all genotypes. The number of plants from each genotype, WT n=6, *proPOLAR::SMR4* n=16, *proPOLAR::SMR8* n=19, *proPOLAR::SMR1* n=13, *proPOLAR::KRP1* n= 14

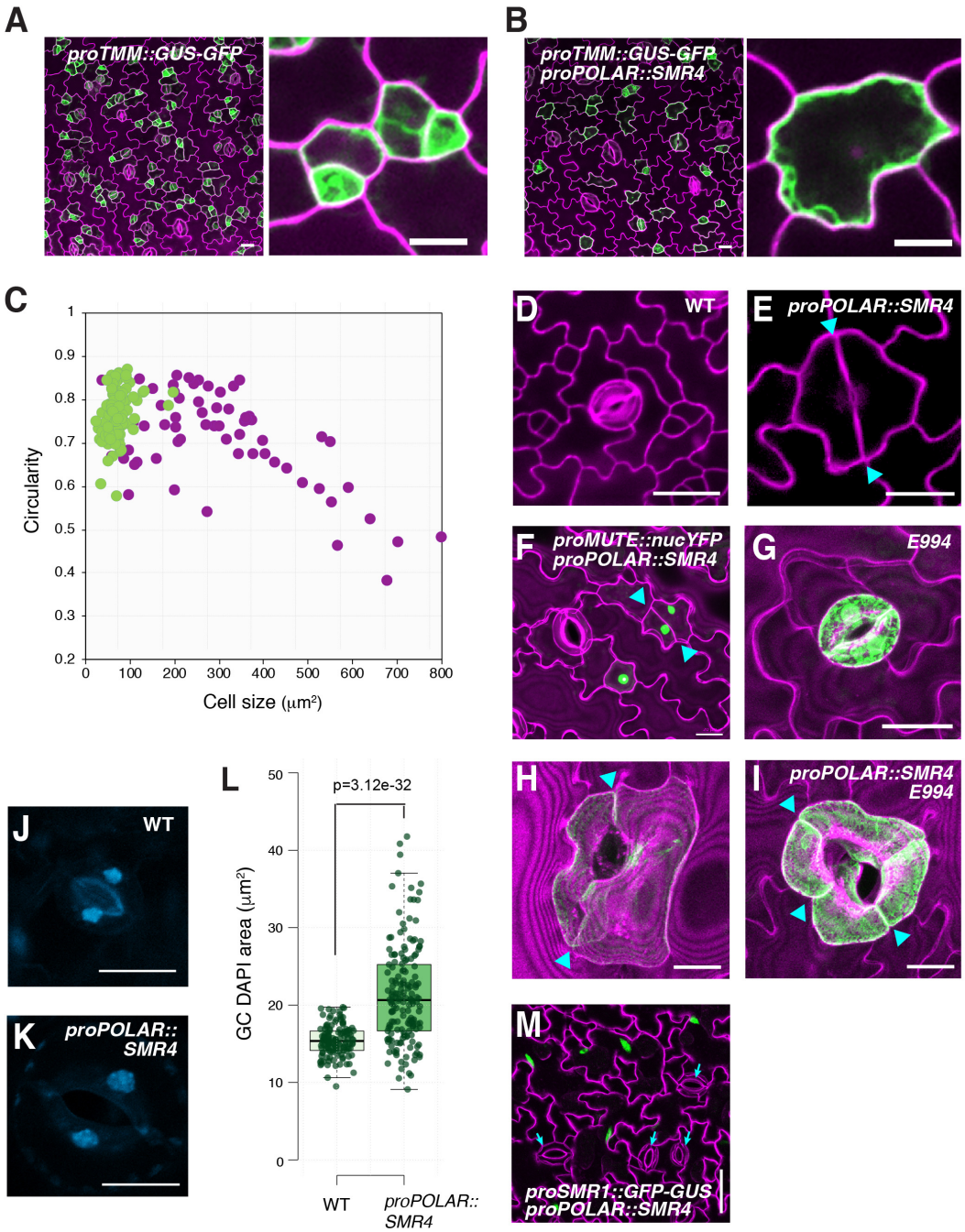

Figure 5. Stomatal-lineage overexpression of *SMR4* reduces proliferative activity of meristemoids

(A) *proTMM::GUS-GFP*, abaxial cotyledon at 4-day post germination stage seedling (4dpg), (B) *proTMM::GUS-GFP* in *proPOLAR::SMR4*, 4dpg, Scale bar: 20 μm. Insets: zoomed stomatal lineage cells expressing GFP. Scale bar, 10 μm

(C) Size distribution vs. circularity of the stomatal lineage precursor cells expressing *proTMM::GUS-GFP* in wild-type (green dots) and *proPOLAR::SMR4* (purple dots) plants.

(D-I) Confocal images of representative stomata: Wild-type stoma (D); Mixed fate stoma developed in *proPOLAR::SMR4* (E); *proMUTE::nYFP* in *proPOLAR::SMR4* (F); Mature GC marker *E994* in wild type (G) and *proPOLAR::SMR4* (H, I). Cyan arrowheads, division site of GCs. Scale bars, 20 μm

(J, K) DAPI stained nuclei in mature GCs from wild-type (J) and *proPOLAR::SMR4* plants (K).

(L) Quantitative analysis of DAPI-stained nuclear area in wild-type (n=128) and *proPOLAR::SMR4* (n=234) GCs. Two-tailed Student t-test was performed. $p=3.12e^{-32}$.

(M) Endoreduplication marker *proSMR1::GFP-GUS* expression in *proPOLAR::SMR4* plants. White arrows indicate enlarged GCs with no GFP expression. Scale bar, 50 μm

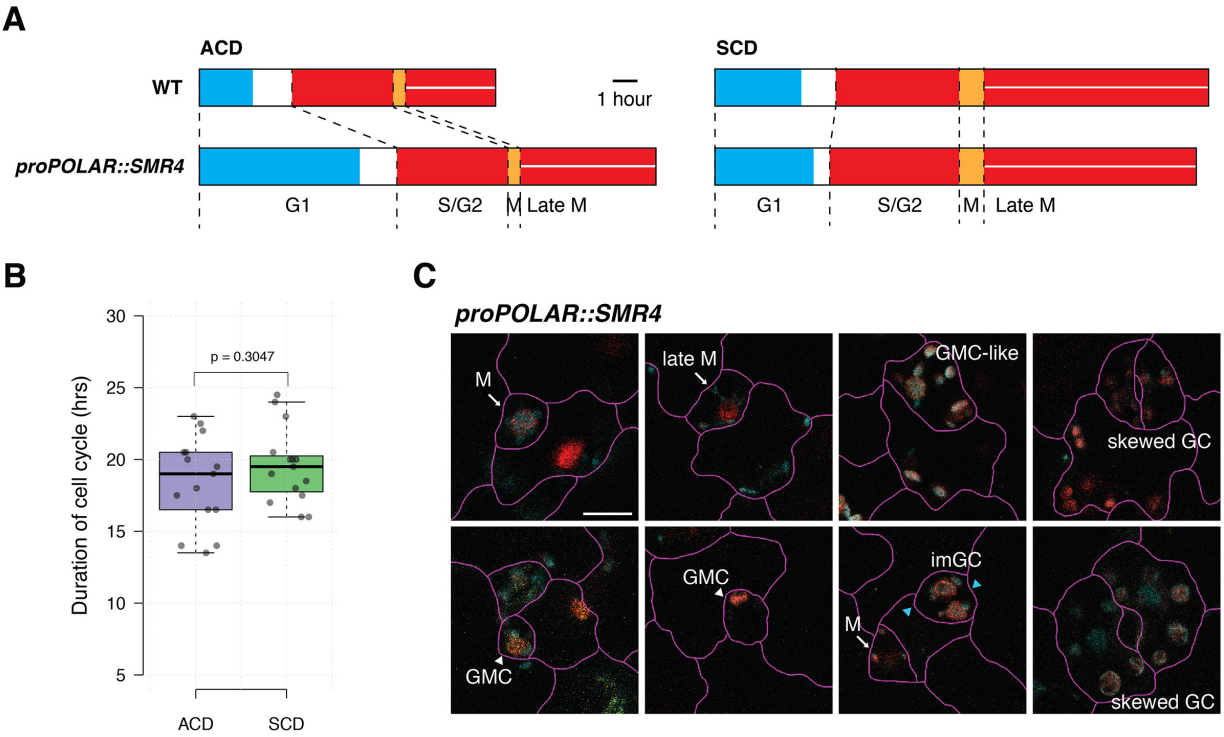

Figure 6. SMR4 slows down the cell cycle progression of ACD through G1 extension

(A) Duration of the cell cycle time of stomatal precursors undergoing ACD and SCD in *proPOLAR::SMR4* lines. n=15 for each cell division mode. Scale bar, 1 hour

(B) Duration of each cell cycle phase calculated from fluorescence intensity of each marker. n=15 for each cell division mode.

(C) Confocal images of stomatal lineage cells from 4-day old cotyledons of a plant expressing three PlaCCI markers. Colors represents the same cell cycle phase as in Fig.1C. Arrow: MMC; Arrowhead: GMC. Scale bar, 10 μm

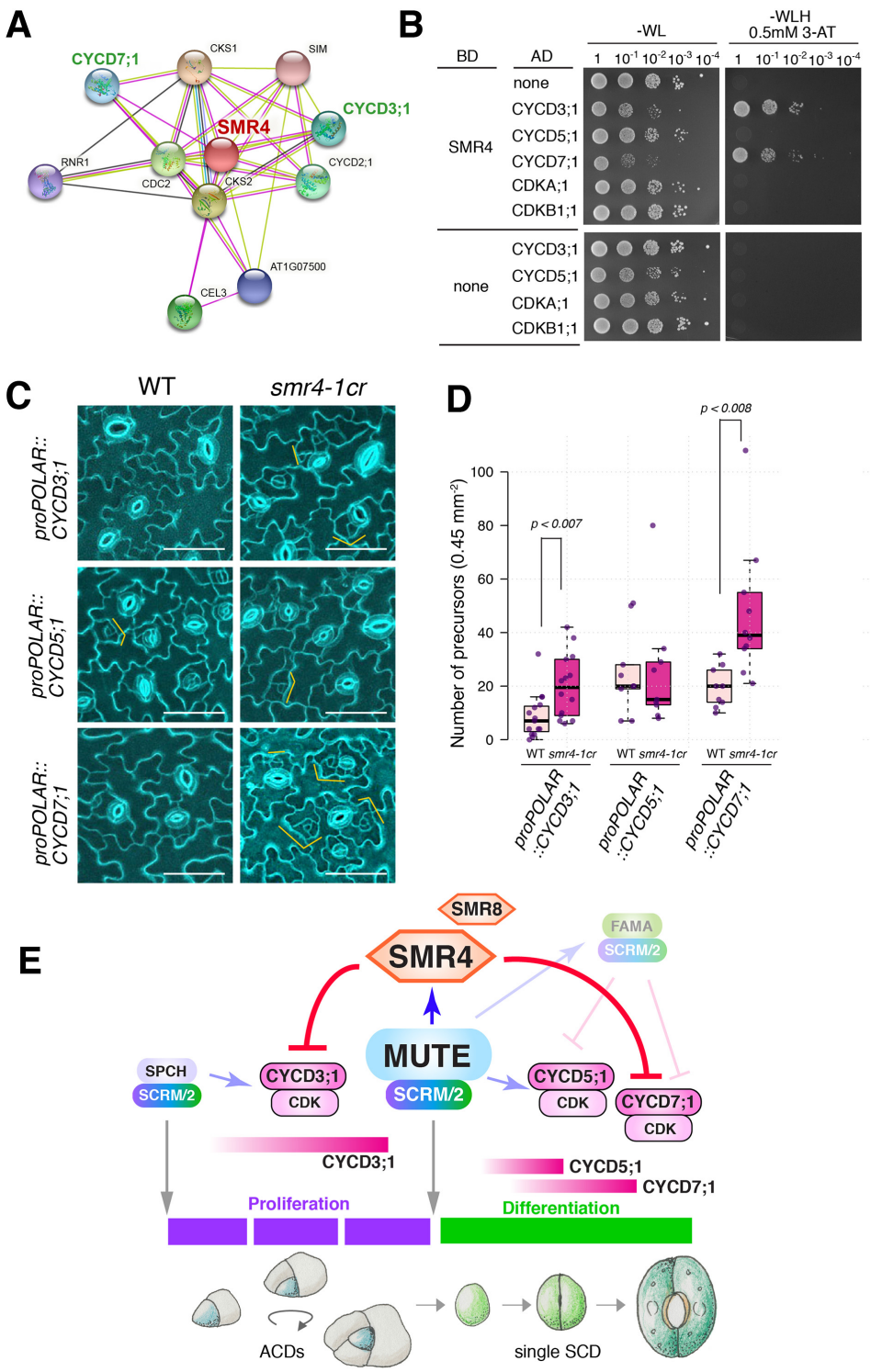

Figure 7. SMR4 decelerates the cell cycle via direct interactions with a selected set of D-type Cyclins

(A) SMR4 interacting proteins visualized by cytoscape.

(B) Yeast-two hybrid assays in which the DNA-binding domain alone (BD) alone or fused to SMR4 were used as bait, and the activation domain alone (AD) or fused to three D-type cyclins, CYCD3;1, CYCD5;1, CYCD7;1 and two cyclin dependent kinases, CDKA;1 and CDKB1;1. Transformed yeast were spotted in 10-fold serial dilutions on appropriate selection media.

(C) Transgenic plants harboring CYCD3;1, CYCD5;1 and CYCD7;1 driven by *POLAR* promoter in wild type and *smr4-1cr.* Scale bar: 50 μm

806 (D) Quantification of stomatal precursor cells (meristemoids and GMC). Epidermal cells were counted
807 from abaxial cotyledon of 7 dpg seedling. Mann-whitney test was performed. P-value of statistically
808 significant pair was marked on top of the boxplot. Independent T1 transgenic plants were analyzed, the
809 number of plants used as follows. *proPOLAR::CYCD3*;1: n=15, *proPOLAR::CYCD3*;1 *smr4-1cr*: n=14,
810 *proPOLAR::CYCD5*;1: n=9, *proPOLAR::CYCD5*;1 *smr4-1cr*: n=9. *proPOLAR::CYCD7*;1: n=9,
811 *proPOLAR::CYCD7*;1 *smr4-1cr*: n=10. *proPOLAR::CYCD7*;1: n=12, *proPOLAR::CYCD7*;1 *smr4-1cr*:
812 n=12
813 (E) Schematic model. SPCH·SCRM/2 module initiates and sustains ACD and MUTE·SCRM/2 trigger
814 SCD (grey arrows) by transcriptionally activating *CYCD3;1* and *CYCD5;1* (shaded blue arrows),
815 respectively. MUTE directly up-regulates *SMR4* transcription (Blue arrow). SMR4 (and SMR8 in part)
816 suppress the activity of CYCD3;1 and CYCD7;1 complexed with CDKs, (red line), but not CYCD5;1, to
817 terminate ACD mode and ensure faithful progression of SCD.
818

819